American Mineralogist, Volume 81, pages 611–624, 1996

In situ X-ray diffraction of aragonite and dolomite at high pressure and high temperature: Evidence for dolomite breakdown to aragonite and magnesite

ISABELLE MARTINEZ,* JIANZHONG ZHANG, AND RICHARD J. REEDER

Center for High Pressure Research and Department of Earth and Space Sciences, State University of New York, Stony Brook, New York, 11794-2100, U.S.A.

ABSTRACT

Energy-dispersive X-ray powder diffraction spectra have been collected for aragonite ($CaCO_3$) and dolomite [$CaMg(CO_3)_2$] at high pressure and high temperature, using synchrotron radiation and a cubic multi-anvil apparatus. Unit-cell volumes were measured up to 7 GPa and 1073 K along several isothermal paths. This study has confirmed previously determined but still debated values of the bulk incompressibilities at 298 K [65.4(5) GPa for aragonite and 90.7(7) GPa for dolomite] and thermal expansivities at 1 bar [$\langle\alpha\rangle_{298-1000\ K} = 6.7(5)\ 10^{-5}\ K^{-1}$ for aragonite and $\langle\alpha\rangle_{298-1000\ K} = 4.1(5)\ 10^{-5}\ K^{-1}$ for dolomite]. In addition, new equation-of-state parameters were measured: $(\partial K/\partial T)_P$ [−0.013(2) and −0.025(4) GPa/K for aragonite and dolomite, respectively] and K'_0 [2.7(7) and 2.3(5) for aragonite and dolomite, respectively]. We suggest that these equation-of-state parameters could be used in the calculation of high-temperature, high-pressure thermodynamic properties of these carbonates.

At pressures exceeding 5 GPa, we observed that dolomite breaks down to aragonite and magnesite. We used the equation-of-state parameters measured in this study to calculate the position of the equilibrium curve: dolomite → aragonite + magnesite. This reaction could be important in the ultra-high-pressure metamorphism of carbonates. This decomposition reaction also provides a useful test of thermodynamic data sets of carbonates at high pressures and temperatures.

INTRODUCTION

To understand the stability of carbonates in the deep Earth as well as the CO_2 outgassing caused by meteorite impacts on the Earth's surface, it is important to know the physical properties of carbonates at the high pressures and temperatures characteristic of the Earth's mantle and of shock metamorphism. Following earlier work performed at $P < 4$ GPa (Irving and Wyllie 1975; Byrnes and Wyllie 1981), several experiments using diamond-anvil cells or multi-anvil apparatus have recently been conducted on carbonates (Katsura and Ito 1990; Canil and Scarfe 1990; Kraft et al. 1991; Williams et al. 1992; Biellmann and Gillet 1992; Ross and Reeder 1992; Biellmann et al. 1993a, 1993b; Gillet et al. 1993; Gillet 1993; Fiquet et al. 1994; Redfern et al. 1993; Ross 1994). Most of these studies concluded that, although carbonates break down at high temperature under low-pressure conditions, they remain stable at simultaneous high pressures and high temperatures (e.g., 30 GPa and 2000 K).

More specifically, aragonite and dolomite have been studied at room temperature using high-pressure Raman and infrared spectroscopy (Kraft et al. 1991; Biellmann and Gillet 1992; Gillet et al. 1993) and P up to 30–40 GPa. In the study by Kraft et al. (1991), infrared spectra of dolomite were collected under high pressure and moderate temperature (up to 550 K), and Raman and infrared spectra were obtained from high-pressure samples quenched from high temperatures (800 K for dolomite and 2100 K for aragonite). Neither destabilization reactions nor phase transformations of dolomite or aragonite were reported in these studies. However, in an analytical transmission electron microscopy study of samples quenched from high temperature and pressures between 20 and 50 GPa, Biellmann et al. (1993b) reported the breakdown of dolomite into calcite and magnesite. In the presence of silicates (pyroxenes or olivines), they observed the formation of magnesite owing to dolomite decomposition, in agreement with petrologic work at lower pressures (Kushiro et al. 1975; Wyllie and Huang 1976; Eggler 1978; Wallace and Green 1988) and the high-pressure study of Katsura and Ito (1990). There is now a clear need for quantitative data to characterize the stability relations of these phases and to resolve the apparent contradictions in the literature. In addition to phase-equilibrium studies, an alternative approach for studying the poorly known phase relations of aragonite and dolomite at deep-mantle conditions is to measure their equations of state (EOS) at high pressures and temperatures.

Dynamic high-pressure studies have also been per-

* Present address: Laboratoire de Géologie, Ecole Normale Supérieure de Lyon, 46, allée d'Italie, 69364 Lyon cedex 07, France.

0003–004X/96/0506–0611$05.00

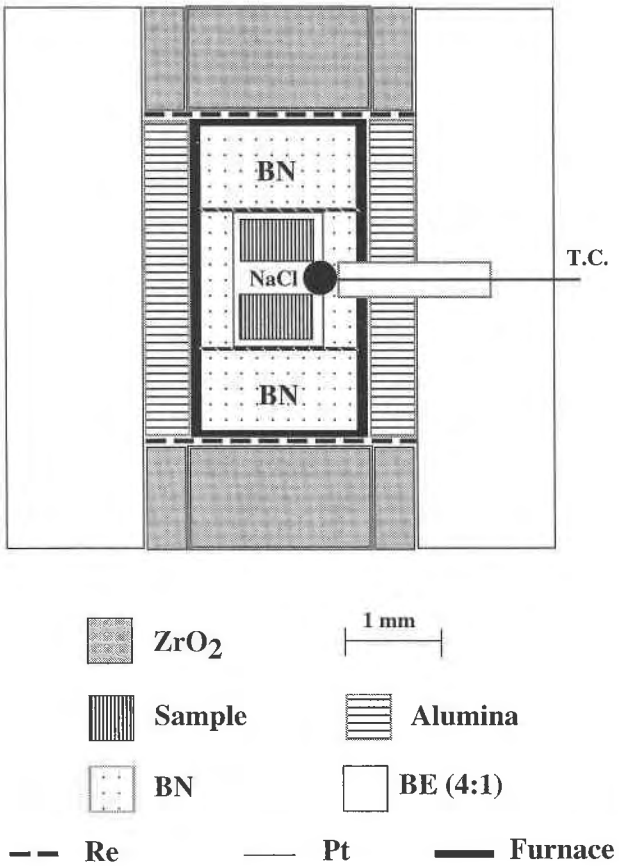

FIGURE 1. Cell assembly used for high P-T X-ray diffraction study in the 6/4 system of the cubic-anvil press (SAM 85). T.C. = thermocouple, BE (4:1) = boron-epoxy mixture with weight ratio 4:1, BN = boron nitride, Re = rhenium foil, Pt = platinum wire, used to provide electrical contact.

formed on carbonates (Kalashnikov et al. 1973; Vizgirda and Ahrens 1982; Kotra et al. 1983; Martinez et al. 1995), and the exact shock conditions necessary to outgas carbonates are still controversial [see, for example, Lange and Ahrens (1983, 1986) and Martinez et al. (1995)]. Because shock temperatures and postshock temperatures are largely determined by EOS parameters, this problem would also benefit from simultaneous high-pressure and high-temperature (high P-T) measurements of carbonates.

Although dynamic EOS are available for dolomitic rocks [compiled in Stöffler (1982)] and for aragonite (Vizgirda and Ahrens 1982), static high-pressure EOS measurements have been confined to room-temperature conditions (Birch 1966; Salje and Viswanathan 1976; Ross and Reeder 1992; Redfern et al. 1993; Ross 1994; Fiquet et al. 1994). Thermal expansion measurements at 1 bar are also available (Salje and Viswanathan 1976; Reeder and Markgraf 1986). So far, no high P-T EOS measurements have been performed on carbonates. In this study, we report the high P-T EOS of dolomite and aragonite as well as the high-pressure breakdown of dolomite to aragonite and magnesite. The high P-T EOS of magnesite is given in a separate study (Zhang et al. 1994).

EXPERIMENTAL TECHNIQUE AND RESULTS

Samples

The aragonite and dolomite samples were selected from pure single crystals from Eugui, Spain. The unit-cell parameters of the aragonite sample used in this work, refined at ambient conditions (P = 1 bar, T = 298 K), are a = 4.967(3), b = 7.961(3), c = 5.744(4) Å, in reasonably good agreement with the values given on the JCPDS card (5-453) of a = 4.959, b = 7.96, c = 5.741 Å. The a and c unit-cell parameters of dolomite at room pressure and room temperature are a = 4.804(2) and c = 15.99(1) Å, comparing well with the data from Ross and Reeder (1992), a = 4.8064(5) and c = 16.006(2) Å, for the same dolomite sample. Eugui dolomite has been used in several other studies (Barber et al. 1981; Reeder 1983; Reeder and Markgraf 1986). The 1 bar room-temperature work by Reeder and Wenk (1983) shows that the composition, $Ca_{1.001}Mg_{0.987}Fe_{0.010}Mn_{0.002}(CO_3)_2$, and cation ordering are nearly ideal. Moreover, transmission electron microscopy shows that Eugui dolomite is homogeneous, with very low density of dislocations (Barber et al. 1981; Reeder and Wenk 1983). Over the P-T range investigated in this study, it is unlikely that cation disorder ever occurred in the sample, even at the highest temperature of 1173 K. It has been shown that no significant disorder occurs in dolomite at 1 bar below 1173 K (Reeder 1983); moreover, at 1 GPa, complete disorder occurs at temperatures exceeding 1400 K (Reeder and Nakajima 1982).

High-pressure, high-temperature diffraction experiments

The high-pressure, high-temperature experiments were performed in a DIA-type, cubic anvil apparatus (SAM-85) operated at the superconductor wiggler synchrotron radiation beamline (X17B) of the National Synchrotron Light Source at Brookhaven National Laboratory. In these experiments the second-stage anvils were made of tungsten carbide, with 4 × 4 mm² square truncations, and the pressure medium was a 6 mm edge cube made of amorphous boron epoxy. Figure 1 is a schematic diagram of the cell assembly used in this system. The powdered sample, together with a layer of NaCl-BN powder mixture, was placed in a boron nitride sleeve in an amorphous carbon furnace. The EOS of NaCl (Decker 1971) was used to determine the pressure at any given temperature, whereas BN was used to prevent recrystallization of the salt during heating. Alumina sleeves and zirconia disks were used to separate the furnace from the pressure medium and the anvils; electrical contact between furnace and anvils was achieved with platinum wires and rhenium discs. A dc power supply was used to provide constant heating, and temperatures were directly measured

in the sample with a W5%Re-W26%Re thermocouple. Pyrophyllite gaskets were used to protect the thermocouple. Previous studies have focused on the characterization of the sample environment both in terms of pressure and temperature gradients (Weidner et al. 1992). In those studies, the maximum temperature gradient at high temperatures (>900 K) and along a vertical axis was estimated to be 20 K from top to bottom of the cell assembly. However, this temperature gradient can be considered a maximum because X-ray diffraction spectra are collected on the portion of the sample closest to the thermocouple junction. As shown by Weidner et al. (1992), pressure gradients are negligible throughout the cell, especially when differential stresses are relaxed during and after heating.

The incident X-ray beam was collimated with 100 μm slits in the vertical direction and 200 μm slits in the horizontal direction. Energy-dispersive X-ray diffraction patterns were collected with a solid-state Ge detector, placed at a fixed 2θ angle of 7.5°, with a mean acquisition time of 200 s. The multichannel analyzer was calibrated before and after the experiment for both energy and 2θ position. The energy calibration and calculation of the 2θ angle were made in a one-step procedure (program "autocal") using characteristic fluorescence lines of molybdenum and lead, as well as the positions of diffraction lines from an assemblage of standards, Si, Al_2O_3, and MgO. This calibration is accurate in the 25–75 keV energy range. During an experiment, the drift in 2θ and energy calibration did not exceed 0.05% and is thus considered as negligible.

The P-T paths followed in the experiments are shown in Figures 2a and 2b for aragonite and dolomite, respectively. The sample was first compressed at room temperature. Temperature was then increased slowly at constant ram load, leading to a decrease of the sample pressure because of both relaxation processes in the cell and gasket flow. The sample was then cooled; the cell pressure decreased again because of the loss of thermal pressure. Heating and cooling cycles were then repeated for several ram loads. After the first heating and cooling cycle, increasing temperature led to an increase in cell pressure because the cell had already relaxed. At chosen P and T conditions, reported in Tables 1 and 2 for aragonite and dolomite, respectively, we collected energy-dispersive X-ray spectra for both the sample and the NaCl.

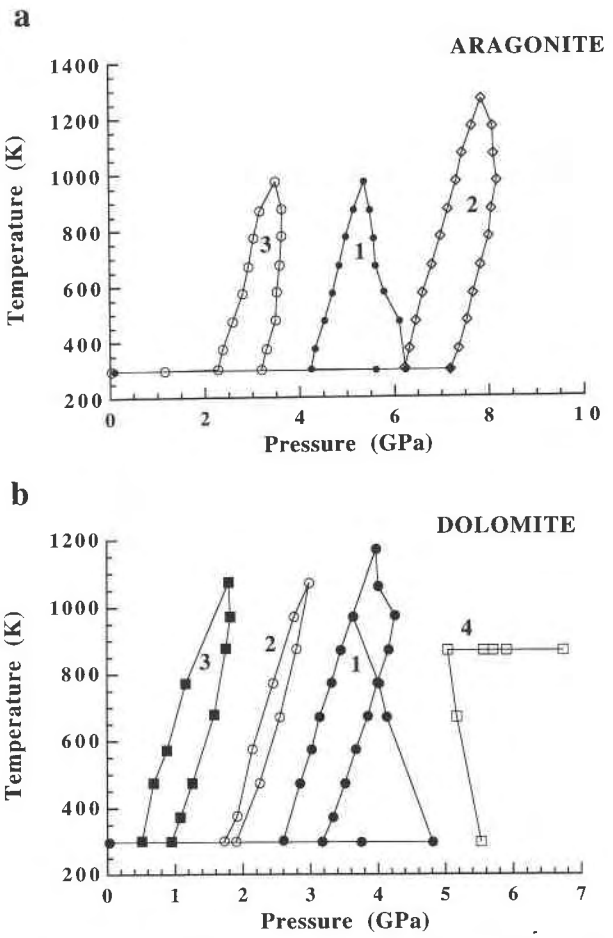

FIGURE 2. Temperature-pressure paths followed during the experiment. The P-T loops are followed counterclockwise. (**a**) For aragonite, three different heating cycles were used, labeled 1–3, up to 8 GPa and 1273 K. (**b**) For dolomite, P-T paths labeled 1–3 were designed for EOS determination, whereas path 4 represents a different experiment used to study the breakdown reaction of dolomite.

Measurements of pressure and nonhydrostatic stress in the cell

The d_{hkl} values of NaCl were obtained by nonlinear least-squares fitting of the recorded X-ray diffraction spectra using a program called GPLS (General Purpose Least Square) and by use of our own calibration program. Then, the unit-cell parameters and volume were refined by a least-squares fitting of the values of $Q_{hkl} = 1/d^2$ using the 111, 200, 220, 222, and 420 diffraction lines. The Decker EOS (Decker 1971) was then used with volume and temperature measurements to determine pressure. The use of other EOS for NaCl (e.g., Birch 1978) does not change the pressure within this pressure and temperature range (Meng et al. 1993), and the precision of the pressure determination is estimated to be better than 0.2 GPa (Meng et al. 1993; Wang et al. 1994).

Nonhydrostaticity in the cell is a very crucial parameter because it affects the determination of both pressure and unit-cell volume of the sample. Nonhydrostatic stresses are removed by heating the sample above the temperature at which it yields and begins to deform plastically. The differential stresses can be estimated quantitatively in the NaCl using the method developed by Weidner et al. (1992) and are given in Tables 1 and 2. In these tables, the differential stress is the difference between the axial and radial stresses, both being negative

TABLE 1. Data acquisition conditions for aragonite

File no.	T (K)	P (GPa)	Differential stress (GPa)
First heating and cooling cycle			
2008	298	6.19	−0.11
2014-16	573	5.77	−0.007
2017-19	673	5.61	+0.01
2020-22	773	5.57	+0.01
2023-25	873	5.49	+0.009
2026-28	973	5.36	−0.01
2029	873	5.17	+0.01
2032-33	773	4.98	+0.02
2034	673	4.85	+0.04
2037-38	573	4.68	+0.04
2039	473	4.53	+0.05
2042-43	373	4.34	+0.08
2044-46	298	4.24	+0.10
Second heating and cooling cycle			
2048	298	5.57	−0.004
2050-51	298	7.14	−0.07
2053	373	7.31	−0.08
2054-56	473	7.50	−0.08
2058	573	7.63	−0.06
2059-61	673	7.81	−0.07
2063	773	7.97	−0.05
2064-66	873	8.06	−0.03
2068	973	8.17	−0.001
2069-71	1073	8.09	−0.02
2073	1173	8.08	−0.01
2074	1273	7.86	+0.01
2076-78	1173	7.66	+0.04
2080	1073	7.46	+0.05
2081-83	973	7.34	+0.04
2085	873	7.13	+0.03
2087	773	6.99	+0.05
2089	673	6.79	+0.05
2090-92	573	6.59	+0.07
2098	473	6.45	+0.04
2100	373	6.31	+0.03
2102-03	298	6.19	+0.01
Third heating and cooling cycle			
2105-6	298	5.08	+0.14
2108-9	298	3.12	+0.11
2111	373	3.34	+0.03
2113	473	3.45	−0.005
2115	573	3.52	+0.01
2117	673	3.59	−0.02
2119	773	3.61	−0.02
2121	873	3.64	+0.01
2123-24	973	3.50	−0.04
2126	873	3.17	−0.08
2128	773	2.98	−0.05
2130-31	673	2.92	+0.05
2133	573	2.79	+0.09
2135	473	2.57	+0.04
2136	373	2.37	+0.10
2139-40	298	2.28	+0.14
2142-43	298	1.15	+0.13
2145	298	0.04	+0.08

TABLE 2. Data acquisition conditions for dolomite

File no.	T (K)	P (GPa)	Differential stress (GPa)
First heating and cooling cycle			
3005	298	0.03	0.00
3006	298	3.75	−0.06
3007	298	4.81	−0.14
3008	673	4.13	+0.001
3011	773	4.02	+0.02
3016	973	3.64	+0.05
3019	298	3.17	−0.02
3022	373	3.33	−0.03
3025	473	3.51	−0.03
3028	573	3.70	−0.03
3031	673	3.85	−0.03
3034	773	3.99	+0.006
3037	873	4.16	−0.01
3040	973	4.28	+0.005
3044	1073	4.00	−0.001
3045	1173	3.98	+0.03
3050	873	3.48	+0.07
3053	773	3.36	+0.04
3056	673	3.16	+0.06
3059	573	3.03	+0.07
3062	473	2.84	+0.04
3065	298	2.58	+0.03
Second heating and cooling cycle			
3066	298	2.38	+0.02
3067	298	1.99	+0.11
3071	298	1.89	+0.14
3074	473	2.23	+0.14
3077	673	2.58	+0.08
3080	873	2.80	+0.07
3083	1073	2.98	+0.04
3086	973	2.79	−0.04
3089	773	2.45	+0.03
3092	573	2.14	+0.02
3095	373	1.86	+0.09
3097	298	1.73	+0.04
3098	298	1.47	+0.03
Third heating and cooling cycle			
3101	298	0.94	+0.17
3104	373	1.08	+0.11
3107	573	1.26	+0.06
3110	673	1.58	+0.01
3113	873	1.75	+0.04
3116	973	1.82	+0.01
3119	1073	1.80	+0.04
3122	773	1.16	+0.02
3125	573	0.88	−0.03
3128	473	0.69	+0.14
Additional experiment			
1006	298	5.53	−0.05
1008	673	5.17	+0.01
1010	873	5.04	+0.01
1012	873	5.57	−0.03
1015	873	5.71	−0.02
1018	873	5.91	−0.04
1020	873	6.74	−0.02

for compression. We generally observe in this cell assembly that compression at room temperature induces negative differential stresses (i.e., axial stress greater than radial stress in absolute values), whereas both cooling and decompression result in positive differential stresses. It appears that in these particular experiments, most of the differential stresses were relaxed when the cell was heated above 700–800 K. When the cell assembly was loaded with materials such as olivine or garnet, higher temperatures were required to remove the nonhydrostatic stress. It should be noted that the absence of differential stress in the NaCl does not necessarily imply zero differential stress in the sample. Weidner et al. (1994) showed that the line width of diffraction peaks in the sample is a good indicator of local deviations from hydrostaticity. This effect is also apparent in carbonates as shown in Figure 3,

which compares the X-ray diffraction spectra of aragonite after pure compression (Fig 3a) and heating at 873 K (Fig 3b). Empirically, differential stress-free spectra are characterized by line widths similar to or even narrower than those in the sample at ambient conditions. Only data with narrow diffraction lines as well as reasonably low nonhydrostaticity measured in the NaCl (typically when the absolute value of the differential stress is smaller than 0.1 GPa) were used for EOS determinations.

Measurement of lattice parameters and EOS

The d_{hkl} values of aragonite and dolomite were obtained by nonlinear least-squares fitting of the recorded X-ray diffraction spectra and our own calibration program. Then, the unit-cell parameters and volume were refined by least-squares fitting the values of $Q_{hkl} = 1/d^2$ (program "celrf") using 10–14 and 6–8 diffraction lines for aragonite and dolomite, respectively. For aragonite we used 111, 021, 121, 012, 200, 031, 112, 130, 022, 211, 221, 202, 132, and 113; and for dolomite we used $10\bar{1}4$, 0006, $01\bar{1}5$, $11\bar{2}0$, $11\bar{2}3$, $20\bar{2}2$, $01\bar{1}8$, and $11\bar{2}6$. Unit-cell volumes and lattice parameters are reported in Tables 3 and 4 for aragonite and dolomite, respectively. Some of the aragonite data points, obtained with calcite as a starting material, loaded in the same cell and transformed in situ during the experiment, are also reported in Table 3. This calcite was loaded a few millimeters above the aragonite. The very small differences in unit-cell parameters and volume measurements between these two sets of data confirm the small pressure and temperature gradients in the cell assembly.

Breakdown of dolomite into aragonite and magnesite

In our first attempt to determine the high P-T EOS of dolomite, we compressed the sample to 8 GPa and heated it. Above 673 K (7.2 GPa), the X-ray diffraction spectra changed dramatically (Figs. 4a and 4b); aragonite and magnesite peaks appeared. At 973 K (7 GPa), all dolomite peaks had disappeared, indicating that the breakdown of dolomite into aragonite and magnesite was complete (Fig. 4c). The unit-cell volumes of aragonite and magnesite in the assemblage are shown in Table 5. They differ only marginally from the unit-cell volumes of pure magnesite, also measured in the same experiment, and those of pure aragonite, determined in a separate experiment at similar conditions. This suggests that the amounts of Mg in aragonite and of Ca in magnesite are very low because the unit-cell parameters of the two phases would have been significantly affected otherwise. In Figure 4, it is interesting to note that the diffraction lines of the new phases are sharper than those of the dolomite, suggesting that magnesite and aragonite grains grew in an environment that was relatively free of differential stresses. In a second experiment performed to locate the breakdown conditions more precisely, we followed a different P-T path (path 4 in Fig. 2b). Dolomite was compressed to P = 5.5 GPa, heated to 873 K (P = 5 GPa), and then recompressed at constant temperature until the breakdown reaction was observed. Onset of the decomposition occurred at 5.7 GPa after these conditions were maintained for more than 90 min. Further compression at 873 K up to 7.4 GPa did not significantly change the proportions between reacted and unreacted material. It was necessary to heat the sample to 1073 K to complete the reaction, suggesting that the breakdown kinetics are quite sluggish at conditions close to equilibrium. For the same reason, attempts to reverse the breakdown reaction at 1073 K and lower pressure suffered kinetic problems.

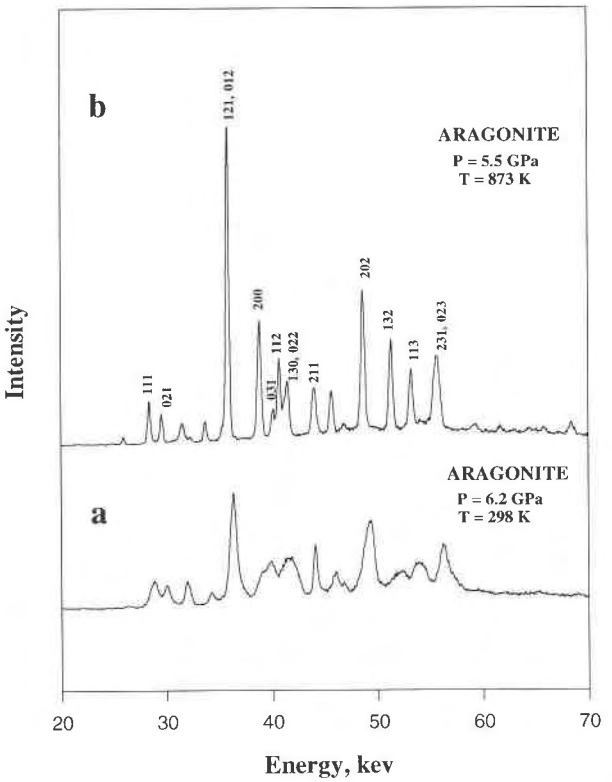

Figure 3. Selected energy-dispersive X-ray diffraction spectra of aragonite at the indicated pressure and temperature. (a) The compressed sample at room temperature (P = 6.2 GPa) shows broad peaks, whereas (b) peaks become sharper when sample is heated above 873 K. The pressure decrease between the room-temperature and the 873 K spectra is due to relaxation processes in the cell assembly.

Discussion

Methods for EOS data processing

Isothermal Birch-Murnaghan equation of state. The measured unit-cell volumes of aragonite and dolomite were fitted along isothermal curves with a Eulerian finite-strain Birch-Murnaghan EOS (Fig. 5):

$$P = \tfrac{3}{2}K_{0,T}[(V_{0,T}/V)^{7/3} - (V_{0,T}/V)^{5/3}]\cdot\{1 + \tfrac{3}{4}(K'_{0,T} - 4)[(V_{0,T}/V)^{2/3} - 1]\}. \quad (1)$$

TABLE 3. Unit-cell volumes and lattice parameters used in the determination of EOS parameters for aragonite

File no.	P (GPa)	Unit-cell V (Å³)	dV* (Å³)	a (Å)	b (Å)	c (Å)
			T = 298 K			
2005	0.00	227.14	0.18	4.967	7.961	5.744
2105	5.10	213.08	0.11	4.896	7.819	5.566
2106**	5.10	212.97	0.15	4.898	7.786	5.584
2108	3.18	218.52	0.20	4.914	7.877	5.645
2109**	3.18	217.05	0.12	4.907	7.856	5.629
2046	4.24	214.43	0.06	4.901	7.814	5.599
2044**	4.24	213.93	0.06	4.898	7.804	5.596
2102	6.22	210.03	0.01	4.88	7.762	5.544
2103**	6.22	210.23	0.19	4.881	7.755	5.553
2050	7.14	206.81	0.15	4.853	7.7164	5.523
2051**	7.14	207.41	0.14	4.861	7.723	5.525
			T = 373 K			
2042	4.33	214.69	0.09	4.899	7.817	5.605
2043**	4.33	214.33	0.05	4.899	7.809	5.602
2053**	7.36	207.65	0.12	4.854	7.73	5.534
2100**	6.32	210.45	0.19	4.884	7.758	5.554
2111**	3.30	217.82	0.02	4.914	7.866	5.635
			T = 473 K			
2039**	4.53	214.97	0.03	4.903	7.815	5.61
2056	7.54	207.63	0.13	4.86	7.72	5.53
2054**	7.54	208.1	0.06	4.86	7.73	5.54
2098**	6.46	210.9	0.11	4.884	7.76	5.56
2113**	3.49	218.37	0.09	4.924	7.856	5.64
			T = 573 K			
2014	5.78	213.64	0.13	4.895	7.815	5.584
2016**	5.78	214.27	0.19	4.899	7.810	5.600
2037	4.70	215.85	0.1	4.902	7.829	5.624
2038**	4.70	215.63	0.04	4.906	7.822	5.619
2058**	7.67	208.4	0.08	4.862	7.733	5.543
2092	6.60	211.11	0.14	4.880	7.781	5.559
2090**	6.60	211.22	0.10	4.892	7.762	5.562
2115**	3.52	219.28	0.10	4.927	7.866	5.657
			T = 673 K			
2019	5.60	214.67	0.10	4.900	7.817	5.604
2017**	5.60	214.21	0.05	4.899	7.811	5.598
2034**	4.84	216.17	0.15	4.900	7.831	5.632
2061	7.83	208.5	0.12	4.870	7.723	5.544
2059**	7.83	209.07	0.08	4.867	7.735	5.553
2089**	6.80	211.71	0.09	4.894	7.766	5.570
2117**	3.59	220.97	0.17	4.934	7.878	5.684
			T = 773 K			
2020	55.75	215.27	0.10	4.898	7.821	5.619
2022**	55.75	215.65	0.09	4.903	7.825	5.620
2032	49.87	216.98	0.16	4.902	7.842	5.644
2033**	49.87	216.77	0.18	4.903	7.837	5.641
2063**	80.07	209.45	0.07	4.875	7.738	5.552
2087**	69.86	212.34	0.09	4.894	7.768	5.585
2119**	36.27	222.32	0.13	4.947	7.888	5.697
			T = 873 K			
2025	5.49	216.88	0.10	4.902	7.839	5.645
2023**	5.49	216.73	0.11	4.903	7.835	5.642
2029**	5.16	217.51	0.16	4.905	7.847	5.650
2066	8.06	210.28	0.10	4.883	7.748	5.559
2064**	8.06	210.14	0.05	4.879	7.747	5.559
2085**	7.15	212.74	0.09	4.897	7.774	5.588
2121**	3.63	222.85	0.12	4.939	7.899	5.711
			T = 973 K			
2026	5.36	218.05	0.26	4.912	7.834	5.667
2028**	5.36	217.91	0.17	4.905	7.759	5.571
2068	8.18	211.31	0.09	4.888	7.759	5.571
2083	7.33	213.39	0.17	4.896	7.789	5.595
2081**	7.33	213.25	0.09	4.889	7.785	5.603
2124	3.50	224.71	0.14	4.944	7.925	5.736
2123**	3.50	224.51	0.14	4.945	7.916	5.735
			T = 1073 K			
2071	8.12	212.55	0.13	4.893	7.768	5.592
2069**	8.12	212.33	0.04	4.892	7.766	5.588
2080	7.46	213.89	0.09	4.894	7.785	5.614
			T = 1173 K			
2073**	8.10	213.56	0.19	4.889	7.777	5.616
2078	7.66	214.38	0.11	4.898	7.791	5.617
2076**	7.66	213.93	0.09	4.897	7.777	5.617
			T = 1273 K			
2074**	7.86	214.59	0.12	4.886	7.787	5.640

* dV = uncertainty of the fit.
** Starting material = calcite; for other data points, starting material = aragonite.

The three parameters $V_{0,T}$, $K_{0,T}$, and $K'_{0,T}$ (the volume, the bulk modulus, and the pressure derivative of the bulk modulus, respectively) were derived from this equation, all at 1 bar and at the temperature of the specific isotherm. In the present study, the investigated compression range combined with the relatively few data points for each isotherm did not allow us to determine all three parameters independently and with reasonable accuracies. We therefore decided to adopt the common assumption that $K'_{0,T}$ is a constant equal to 4, which is identical to restricting the Birch-Murnaghan EOS to second order (e.g., Poirier 1991). The $K_{0,T}$ and $V_{0,T}$ parameters were thus determined for temperatures ranging from 298 to 973 K and are reported in Table 6 together with the uncertainties of the fit to a second-order Birch-Murnaghan equation. The temperature dependence of $K_{0,T}$ can be simply described by

$$K_{0,T} = K_{0,298\ \mathrm{K}} + (\mathrm{d}K_{0,T}/\mathrm{d}T)\,(T - 298) \qquad (2)$$

as is shown in Figure 6, in which the average value of $\mathrm{d}K_{0,T}/\mathrm{d}T$ deduced from a linear fit as well as the standard deviation to the fit are given. It is also possible (Fig. 7) to obtain an average thermal expansion coefficient $\langle\alpha\rangle_{298-1000\ \mathrm{K}}$ between 298 and 1000 K, defined by

$$V_{0,T} = V_{0,298\ \mathrm{K}}\,\{1 + \langle\alpha\rangle_{298-1000\ \mathrm{K}}\,[T\,(\mathrm{K}) - 298]\}. \qquad (3)$$

The difference between this linear fit and a more exact exponential fit is negligible in the temperature range considered in the study. Values of $K_{0,T}$, $K'_{0,T}$, $\mathrm{d}K_{0,T}/\mathrm{d}T$, and $\langle\alpha\rangle_{298-1000\ \mathrm{K}}$ are summarized in Table 7, along with EOS parameters from earlier work for comparison. Strictly speaking, the parameter $\mathrm{d}K_{0,T}/\mathrm{d}T$ is different from the usual $(\partial K/\partial T)_P$, but it is likely that this difference is small and contained within the experimental error bars.

High-temperature Birch-Murnaghan equation of state. To crosscheck the EOS analysis, we also performed for each phase an inversion of the whole set of experimental data, on the basis of the third-order Birch-Murnaghan

TABLE 4. Unit-cell volumes and lattice parameters used in the determination of EOS parameters for dolomite

File no.	P (GPa)	Unit-cell V (Å³)	dV* (Å³)	a (Å)	c (Å)
		T = 298 K			
3005	0.03	319.77	0.35	4.804	15.997
3019	3.17	310.55	0.11	4.7706	15.757
3065	2.58	312.05	0.26	4.774	15.810
3071	1.89	314.60	0.15	4.7854	15.864
3097	1.73	315.32	0.18	4.7867	15.891
1006	5.53	303.40	0.18	4.7515	15.518
		T = 373 K			
3022	3.33	310.16	0.38	4.7666	15.763
3095	1.86	315.68	0.23	4.786	15.914
3104	1.08	318.44	0.19	4.7988	15.967
		T = 473 K			
3107	1.26	318.80	0.14	4.7994	15.982
3025	3.51	311.00	0.27	4.7722	15.769
3062	2.84	313.24	0.11	4.7792	15.836
3074	2.23	315.26	0.11	4.7873	15.884
		T = 573 K			
3028	3.70	311.34	0.31	4.7726	15.783
3125	0.88	320.88	0.18	4.8032	16.06
3092	2.14	316.38	0.17	4.789	15.929
3059	3.03	313.40	0.10	4.7784	15.849
		T = 673 K			
1008	5.17	306.95	0.29	4.7616	15.633
3031	3.85	311.66	0.25	4.7746	15.786
3056	3.16	313.70	0.13	4.7784	15.864
3077	2.58	316.0	0.12	4.7886	15.913
3110	1.59	319.78	0.13	4.8014	16.017
		T = 773 K			
3034	3.10	311.93	0.33	4.7746	15.800
3053	3.36	314.21	0.10	4.7803	15.877
3089	2.45	317.17	0.29	4.7908	15.957
3122	1.16	322.07	0.11	4.8067	16.096
		T = 873 K			
1010	5.04	309.13	0.3	4.7654	15.718
1012	5.57	307.80	0.33	4.7608	15.681
1015	5.71	306.70	0.38	4.7598	15.632
1018	5.91	306.21	0.33	4.7548	15.639
1020	6.74	303.22	0.51	4.7392	15.589
3037	4.16	312.21	0.27	4.7748	15.813
3050	3.48	314.73	0.11	4.7807	15.901
3080	2.80	317.33	0.08	4.7917	15.959
3113	1.75	321.14	0.12	4.8047	16.063
		T = 973 K			
3016	3.64	314.88	0.16	4.7824	15.898
3040	4.28	313.87	0.43	4.7808	15.857
3086	2.80	318.33	0.15	4.7939	15.994
3116	1.82	322.42	0.15	4.8068	16.114
		T = 1073 K			
3044	4.00	315.23	0.36	4.780	15.926
3083	2.10	319.01	0.31	4.796	16.016
3119	1.80	324.43	0.25	4.7812	16.178

* dV = uncertainty of the fit.

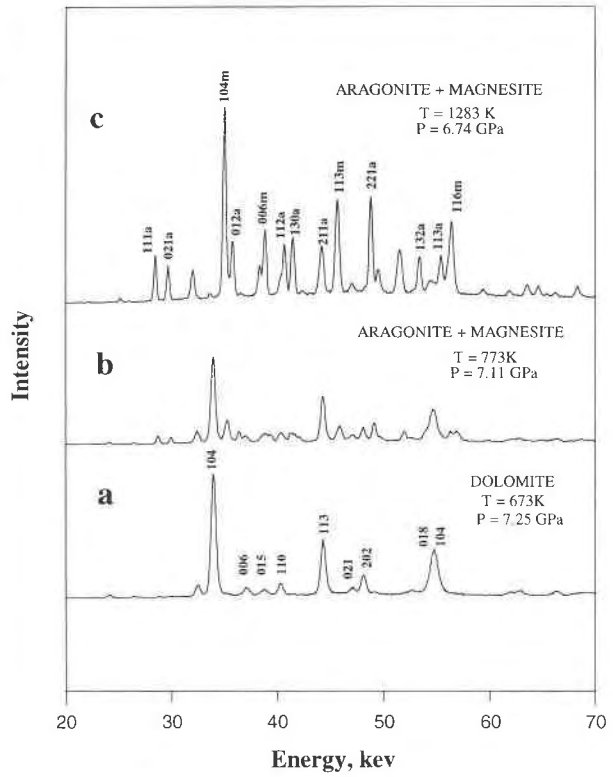

FIGURE 4. Energy-dispersive X-ray diffraction spectra collected during heating of dolomite near 8 GPa. (a) At 673 K, dolomite spectrum remains unchanged, with peaks already quite sharp; (b) at 773 K, some new peaks appear; (c) at 1283 K, the diffraction lines are all indexable for aragonite and magnesite (a and m lines, respectively, on the diffraction spectra); dolomite has been completely transformed.

equation of state at high temperature (HTBM), proposed by Saxena and Zhang (1990). This equation is modified from Equation 1 in the following way: $V_{0,T}$ is written as

$$V(0, T) = V_{0,298\,K}\left\{\exp\left[\int_{298}^{T} \alpha(T)\, dT\right]\right\} \quad (4)$$

with

$$\alpha(T) = \alpha_0 + \alpha_1 T \quad (5)$$

and the isothermal incompressibility is given by Equation 2. To test the sensitivity to the functional forms used in the EOS, other temperature dependencies of α were checked, such as

$$\alpha(T) = \alpha_0 + \alpha_1/T^2. \quad (6)$$

Because of the limited pressure and temperature ranges of this study, $K'_{0,T}$ was assumed to be independent of temperature. With this procedure, six parameters are refined, namely $V_{0,298\,K}$, $K_{0,298\,K}$, $K'_{0,T}$, $dK_{0,T}/dT$, α_0, and α_1, on the basis of 64 data points for aragonite and 42 data points for dolomite. The results of this inversion are shown in Table 7, together with the uncertainty of the fit. They compare very well with the results obtained using the second-order isothermal Birch-Murnaghan EOS (Table 7). Use of a different functional form for α by substituting Equation 6 for Equation 5 did not significantly change the results for the other parameters.

TABLE 5. Determination of unit-cell volume of aragonite and magnesite formed in the dolomite breakdown reaction

P (GPa)	T (K)	Unit-cell V magnesite in mix. (Å³)	Unit-cell V aragonite in mix. (Å³)	Unit-cell V pure magnesite* (Å³)	Calc. unit-cell V of pure aragonite (Å³)**
7.02	873	269.2(6)	212.4(3)	267.2(3)	213.1
6.99	973	267.0(5)	214.0(2)	268.7(1)	214.2
6.86	1073	271.6(6)	215.4(1)	269.6(2)	215.4
6.78	1173	270.7(2)	216.7(2)	272.8(6)	216.4
6.74	1273	274.8(2)	218.2(3)	272.5(1)	217.5

* Measured at the same P-T conditions in the same experiment; see Zhang et al. (1994).

** Calculated from the closest experimental conditions at the same temperature, in pure aragonite experiment, corrected for the pressure difference with a K_T value estimated at these P-T conditions.

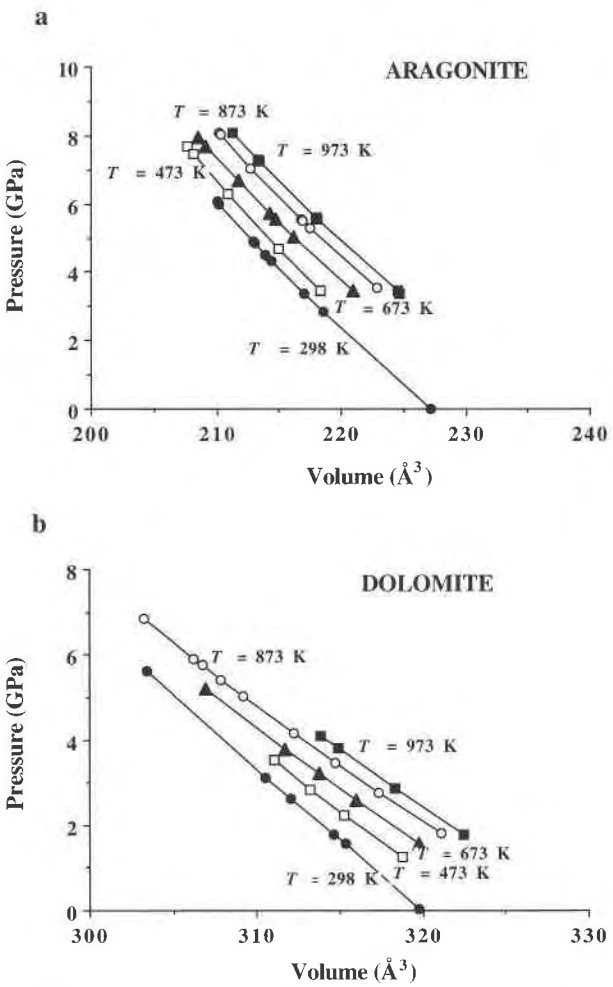

FIGURE 5. P-V diagrams showing unit-cell volume along isotherms. Lines represent best fit of the data, using a third-order Birch-Murnaghan equation of state with $K'_{0,T} = 4$. (**a**) Aragonite sample. At 298 K, the fit of the data gives a value of $K_{0,T}$ = 64.8(4.3) GPa. (**b**) Dolomite sample. At 298 K, the fit of the data gives a value of $K_{0,T}$ = 91(4) GPa.

TABLE 6. Determination of $K_{0,T}$, $V_{0,T}$ along isotherms, assuming $K'_{0,T} = 4$

T (K)	$K_{0,T}$ (GPa)	$\sigma K_{0,T}$* (GPa)	$V_{0,T}$ (Å³)	$\sigma V_{0,T}$** (Å³)
		Dolomite		
298	91.3	3.7	320.6	0.4
373	88.3	9.9	321.6	0.75
473	82	0.25	323.6	0.03
573	83.4	0.4	324.2	0.5
673	74.9	1.53	326.4	0.3
773	79.2	1.3	326.7	0.2
873	70.9	1.4	329.1	0.4
973	75.3	8.6	329.8	1.4
		Aragonite		
298	64.81	3.48	227.5	0.8
373	68.09	4.6	228	0.48
473	62.8	3.8	229.6	0.4
573	60.7	4.7	231.2	0.6
673	55.45	3.16	232.9	0.5
773	54.8	4.09	234.3	0.6
873	55.7	1.8	235.6	0.3
973	54.8	2.51	237.1	0.5

* $\sigma K_{0,T}$ = uncertainty of the second-order Birch-Murnaghan fit.
** $\sigma V_{0,T}$ = uncertainty of the second-order Birch-Murnaghan fit.

Thermal pressure. The thermal pressure formalism has been successfully used to analyze high-temperature EOS data [e.g., Anderson (1984) and his subsequent studies]. The differential thermal pressure is determined by subtracting the pressure at volume V and room temperature obtained using Equation 1 from that measured at the same V but at temperature T. The differential thermal pressure ΔP_{th} is thus the difference between the thermal pressure at T and the thermal pressure at room temperature:

$$\Delta P_{th} = P_{th}(V, T) - P_{th}(V, 298\ \text{K}) = P(V, T) - P(V, 298\ \text{K}). \quad (7)$$

Results of thermal pressure analysis on aragonite and dolomite are shown in Figure 8.

EOS parameters of aragonite and dolomite

Aragonite. Unit-cell volumes of aragonite are shown in Figure 5a along different isothermal curves. The results of the isothermal second-order Birch-Murnaghan analysis are shown in Table 6 and Figures 6a and 7a. The value of $K_{0,298\ K}$ = 64.8 (±4.3) GPa determined in this work is consistent with previously determined values of 64.5 GPa (Birch 1966), 66.7 GPa (Salje and Viswanathan 1976), and 64.5 GPa (Martens et al. 1982). The average thermal expansion coefficient between 298 and 1000 K is $\langle\alpha\rangle_{298-1000\ K}$ = 6.5(1) × 10^{-5} K^{-1}. In the specific case of aragonite, thermal expansion had never been studied over such a wide range of temperature because at ambient pressure aragonite transforms back to calcite upon heating. The value given in Salje and Viswanathan (1976), measured up to 573 K, compares well with our value. A linear fit with Equation 2 suggests that the temperature derivative of the bulk modulus is close to −0.018 GPa/K (Fig. 6a). The analysis using the high-temperature, third-order Birch-Murnaghan EOS confirms these results and provides ad-

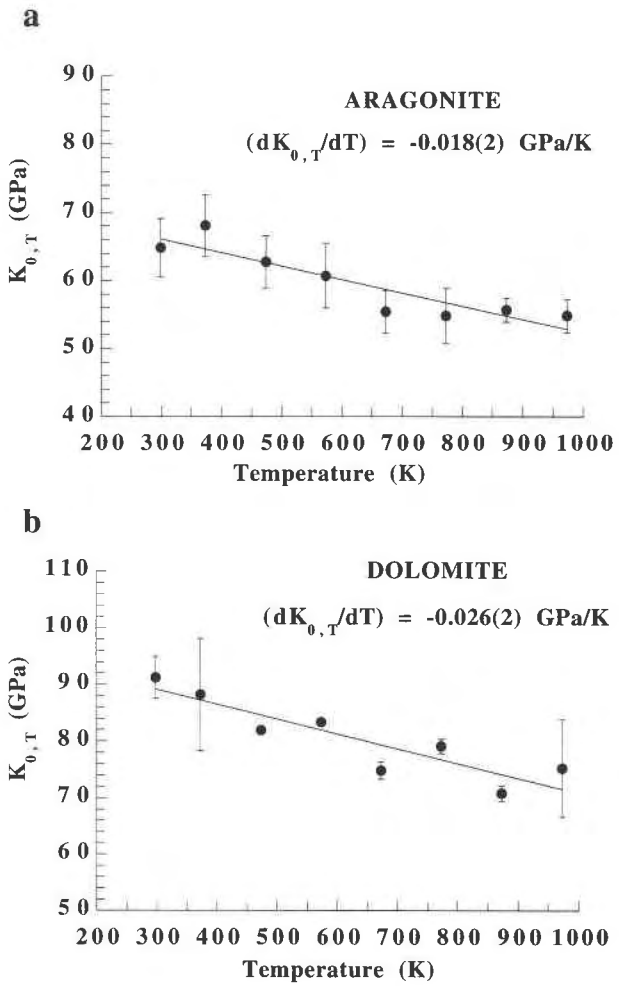

FIGURE 6. Bulk modulus as a function of temperature. Each value of $K_{0,T}$ has been determined from fitting the volume data along an isotherm. A linear fit of these data leads to the value of $dK_{0,T}/dT$ shown for (**a**) aragonite and (**b**) dolomite with $K'_{0,T} = 4$. The numbers in parentheses correspond to residuals of the linear fit.

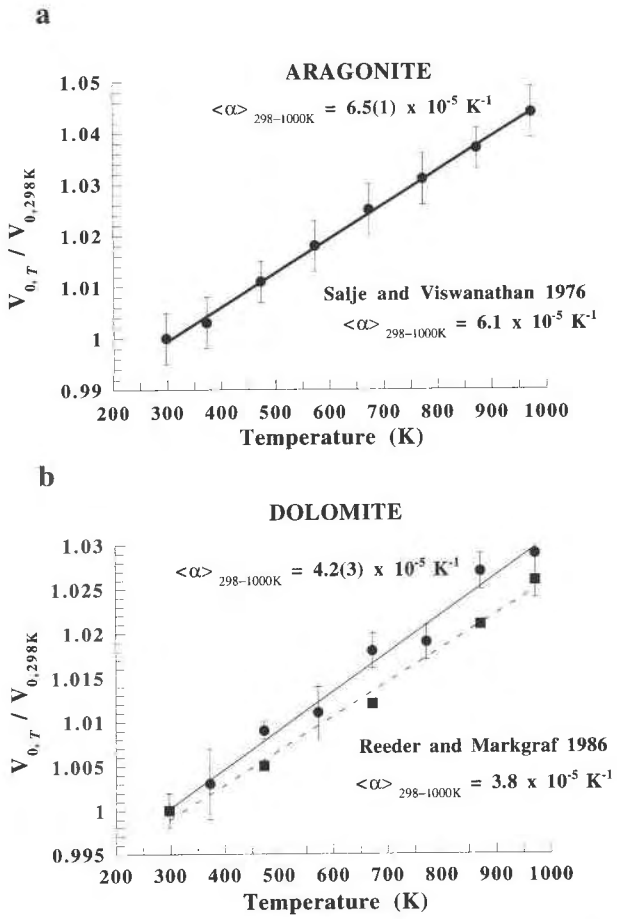

FIGURE 7. $V_{0,T}/V_{0,298\,K}$ as a function of temperature. Each value of $V_{0,T}$ has been deduced from fitting the volume data along isotherms. A linear fit of these data leads to a mean value for thermal expansion for (**a**) aragonite and (**b**) dolomite. Solid squares are data from an earlier 1 bar study (Reeder and Markgraf 1986). The numbers in parentheses correspond to residuals of the linear fit.

ditional evidence that $K'_{0,T}$ is very likely to be <4 (Table 7). The thermal pressure in aragonite at temperatures above 298 K is shown in Figure 8a as a function of temperature. The trend is approximately linear, yielding an average αK value of 0.0039(2) GPa/K, in qualitative agreement with the values of both $\langle\alpha\rangle_{298-1000\,K}$ and $K_{0,298\,K}$ determined above. Within the precision of the present data at a given temperature, it is impossible to detect any significant volume dependence.

Dolomite. The value of $K_{0,298\,K}$ reported in this study [$K_{0,298\,K} = 90.7(7)$, Table 7] is slightly lower than the value of $K_{0,298\,K} = 112.9\ (\pm 2.2)$, with $K'_{0,T} = 4$, reported by Fiquet et al. (1994). The high value of $K_{0,298\,K}$ reported in this room-temperature diamond-anvil cell study might be due to nonhydrostatic conditions that can significantly affect the V measurements. This difference might also be due to the existence of a change in compression mechanism detected at 4 GPa in the study of Fiquet et al. (1994). The small number of data points collected in dolomite in our study at room temperature and pressures exceeding 4 GPa does not allow us to resolve this issue. Our value compares well with $K_{0,298\,K} = 94.1(7)$, $K'_{0,T} = 4$, obtained by Ross and Reeder (1992), and $K_{S0} = 94.9$ GPa derived from single-crystal ultrasonic measurement of Humbert and Plicque (1972). The variations of $K_{0,T}$ and $V_{0,T}$ with temperature are plotted in Figures 6b and 7b. A linear fit with Equation 2 suggests that the temperature derivative of the bulk modulus is close to -0.026 GPa/K (Fig. 6b). The analysis using the high-temperature, third-order Birch-Murnaghan EOS provides a similar value for $dK_{0,T}/dT$ of $-0.025(4)$ GPa/K (Table 7). The average thermal expansion coefficient between 298 and 1000 K, $\langle\alpha\rangle_{298-1000\,K} = 4.2(3) \times 10^{-5}\ K^{-1}$, is in reasonable agreement with the value of $3.79 \times 10^{-5}\ K^{-1}$ determined by Reeder and Markgraf (1986). The inversion with the high-temperature, third-order Birch-Mur-

Table 7. Equation-of-state parameters of aragonite and dolomite

Ref.	$K_{0,T}$ (GPa)	$K'_{0,T}$	$(dK_{0,T}/dT)$ (GPa/K)	$\langle\alpha\rangle_{298-1000\,K}$ ($10^{-5}K^{-1}$)	Method
			Aragonite		
1	64.5	4	—	—	sample dimensions
2	66.66	—	—	6.1	piston displacement
3	64.52	—	—	—	ultrasonic
4	64.8 ± 4.3	4	−0.018(2)	6.5 ± 0.1	X-ray
5*	65.4 ± 0.5	2.7 ± 0.7	−0.013(2)	6.7 ± 0.5	X-ray
				α_0 = 6.5(5)*	X-ray
				α_1 = 3.1(3)*	X-ray
			Dolomite		
6	112.9 ± 2.2	4	—	—	X-ray
	96.0 ± 5.2	10.0 ± 2.2		—	
7	—	—	—	3.8	X-ray
8	94.1 ± 0.7	4	—	—	X-ray
9	94.9–90.2	—	—	—	ultrasonic
3	81.96			—	ultrasonic
4	91 ± 4	4	−0.026(2)	4.2 ± 0.3	X-ray
5*	90.7 ± 0.7	2.3 ± 0.5	−0.025(4)	4.1 ± 0.5	X-ray
				α_0 = 3.8(5)*	X-ray
				α_1 = 5.0(3)*	X-ray

Note: References are as follows: 1 = Martens et al. 1982; 2 = Salje and Viswanathan 1976; 3 = Birch 1966; 4 = this work, second-order B-M; 5 = this work, third-order B-M; 6 = Fiquet et al. 1994; 7 = Reeder and Markgraf 1986; 8 = Ross and Reeder 1992; and 9 = Humbert and Plicque 1972.
* $\alpha = \alpha_0\,(10^{-5}K^{-1}) + \alpha_1\,(10^{-9}K^{-2})T$.

naghan EOS leads to $\langle\alpha\rangle_{298-1000\,K} = 4.1(4) \times 10^{-5}\,K^{-1}$ (Table 7). This latter inversion also shows that $K'_{0,T}$ is significantly <4 (Table 7). Such low values of $K'_{0,T}$ might be a general feature among carbonates, as suggested by magnesite data [$K'_{0,T}$ = 2.2(7), Ross 1994; $K'_{0,T}$ = 2.5(2), Fiquet et al. 1994; $K'_{0,T}$ = 2.3(9), Zhang et al. 1994] and aragonite data [$K'_{0,T}$ = 2.7(7), this study]. Such low values of $K'_{0,T}$ might also have important implications for the thermodynamic properties of carbonates at ultrahigh pressures. The thermal pressure in dolomite, calculated using Equation 7, is shown in Figure 8b, yielding an average αK value of 0.0032(2) GPa/K. At 673, 773, and 973 K, at which enough data points have been collected isothermally, a significant volume dependence of the thermal pressure is observed (Fig. 8c).

Linear compressibilities and thermal expansions of crystallographic axes

Aragonite. The relative compressions a/a_0, b/b_0, and c/c_0 are plotted in Figure 9a for two temperatures, 298 K (solid symbols) and 873 K (open symbols). At room temperature, the c axis of aragonite [mean linear compressibility: 5.8(2) × 10^{-3} GPa^{-1}] is about three times more compressible than the a axis [mean linear compressibility: 2.4(2) × 10^{-3} GPa^{-1}]. The b axis, with a mean linear compressibility of 4.2(2) × 10^{-3} GPa^{-1}, is intermediate between a and c. At higher temperatures, within the precision of the present measurements, the same relative order of the linear compressibilities of a, b, and c is preserved. The relatively high compressibility of the c axis

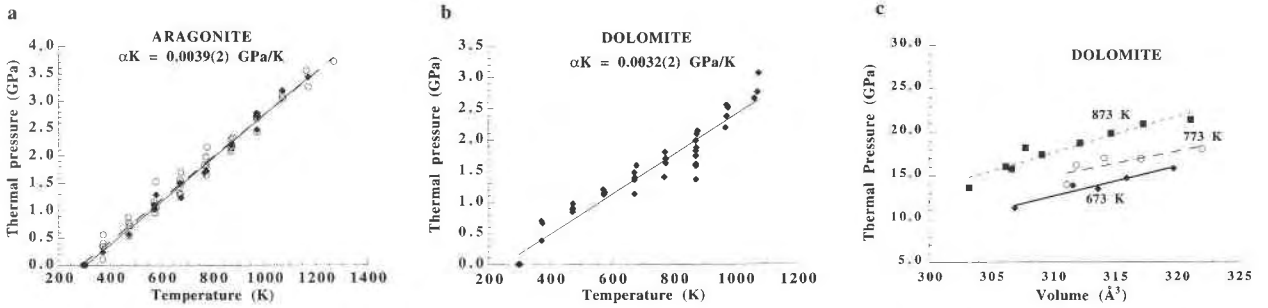

Figure 8. Thermal pressure, calculated using Equation 7, as a function of temperature. (**a**) Aragonite. Open circles and solid diamonds correspond to calcite and aragonite starting material, respectively. Linear fits of these data (shown here as lines) give a mean value for αK = 0.0039(2) GPa/K. (**b**) Dolomite. A mean value for αK = 0.0032(2) GPa/K is deduced by a linear fit (solid line) of the data. (**c**) Dolomite. Thermal pressure as a function of volume at 673, 773, and 873 K, showing volume dependence of thermal pressure at a given temperature.

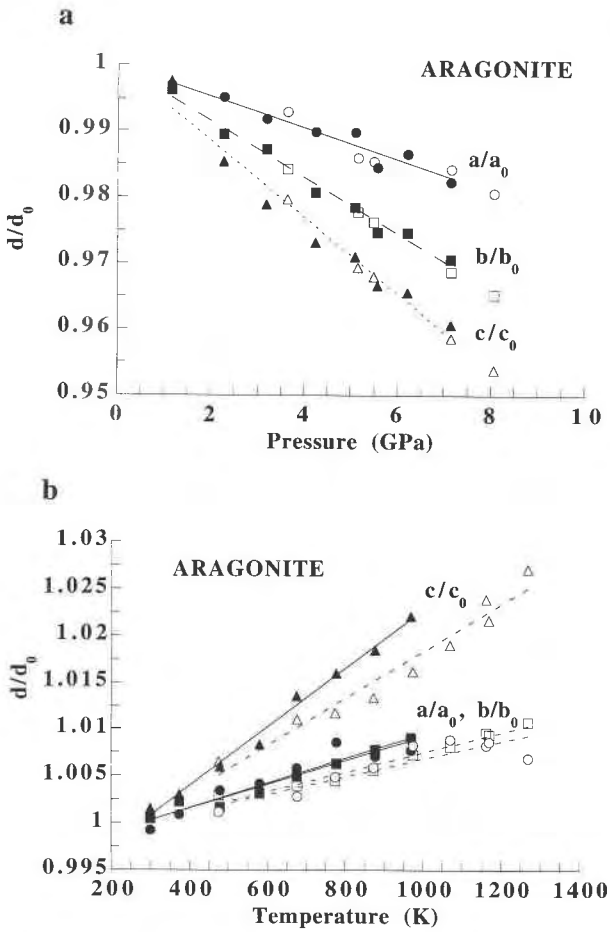

FIGURE 9. (a) Variation of a/a_0, b/b_0, and c/c_0 with pressure in aragonite. Solid symbols correspond to room-temperature data, whereas open symbols show data at 873 K. A linear fit of the room-temperature data (shown by the lines) gives a value of the mean linear compressibilities for the *a*, *b*, and *c* axes. The fits are essentially identical at room temperature and 873 K. (b) Variation of a/a_0 (squares), b/b_0 (circles), and c/c_0 (triangles) with temperature in aragonite. Solid symbols are for 3.5 GPa data and open symbols are for 8 GPa. A linear fit of the data (shown by the lines) gives values for the mean linear thermal expansion coefficients (given in the text).

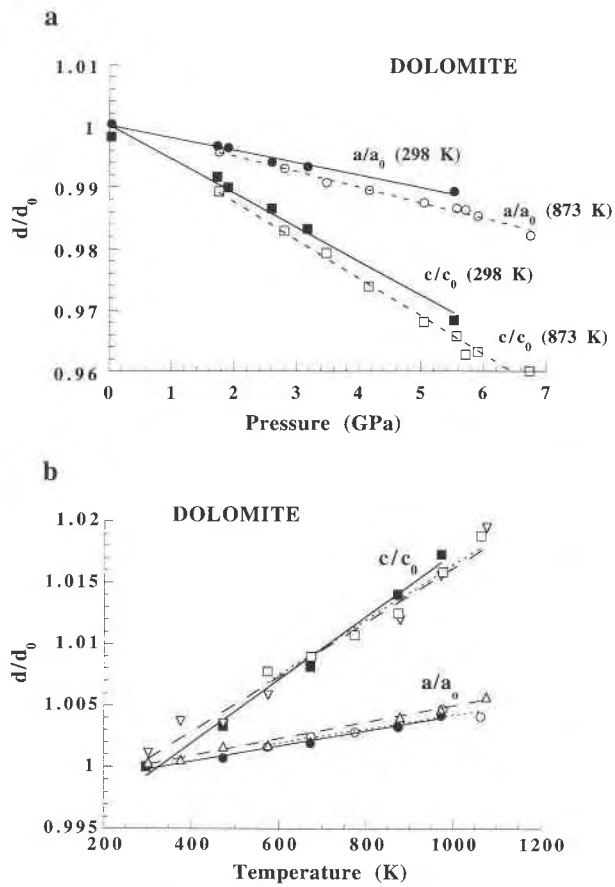

FIGURE 10. (a) Variation of a/a_0 and c/c_0 with pressure in dolomite. Solid symbols correspond to 298 K data, open symbols to 873 K data. Linear fits of the data (solid and dashed lines) give values of the mean linear compressibilities for the *a* and *c* axes (given in the text). (b) Variation of a/a_0 and c/c_0 with temperature in dolomite. Solid symbols represent data at ambient pressure, open triangles show $P = 2$ GPa, and other open symbols show $P = 4$ GPa. Linear fit of the data (solid and dashed lines) give values for the mean linear thermal expansion coefficients (given in the text).

is readily explained by the fact that it is perpendicular to the planar CO_3^{2-} groups and that this direction does not contain short O-O distances.

Isobaric thermal expansivities of crystallographic axes are represented in Figure 9b for pressures of 3.5 and 8 GPa. They were obtained by a simple and small isothermal pressure correction to the experimental points with pressures close to these two values. The average linear thermal expansion coefficients of *a* and *b* between 298 and 1000 K are similar [$<\alpha_{a,b}>_{298-1000\ K} = 1.3(2) \times 10^{-5}\ K^{-1}$ at 3.5 GPa and $<\alpha_{a,b}>_{298-1000\ K} = 1.0(2) \times 10^{-5}\ K^{-1}$ at 8 GPa]. The *c* axis has a mean linear thermal expansion coefficient that is on average three times larger [$<\alpha_c>_{298-1000\ K} = 3.0(2) \times 10^{-5}\ K^{-1}$ at 3.5 GPa and $<\alpha_c>_{298-1000\ K} = 2.5(2) \times 10^{-5}\ K^{-1}$ at 8 GPa]. The decrease of the thermal expansion coefficient with pressure is quite evident for the *c* axis. The relative high thermal expansivity of the *c* axis is related to the same factors giving it a high compressibility. Inverse relation of bond thermal expansivities and bond compressibilities are common, and such relationships often hold for crystallographic axes (e.g., Hazen and Finger 1982).

Dolomite. The relative compressions a/a_0 and c/c_0 at room temperature are plotted in Figure 10a. The abrupt hardening along the *a* axis observed at room temperature by Fiquet et al. (1994) is not seen here probably because only one data point has been collected at room temperature above 4 GPa in this study. Such a hardening is not

TABLE 8. Calorimetric data for magnesite, aragonite, and Eugui dolomite

		$C_p = a + bT + cT^{-2} + dT^{-0.5}$			
$\Delta H^0 f$ (kJ/mol)	S [J/(mol·K)]	a	b ($\times 10^{-5}$)	c	d
		Magnesite			
−1111.8*	65.10**	0.1947**	−0.6081**	287.4**	−2.0738**
		Aragonite			
−1208.16**	88**	0.0842**	4.2844**	−1397.5**	0**
		Eugui-dolomite			
−2328.34†	155.20**	0.3581**	−0.5581**	0**	−3.4347**

* Calculated from Chai and Navrotsky 1993.
** Holland and Powell 1990.
† Calculated from Chai et al. 1995.

detected at 873 K either. The linear compressibilities at 298 K of the a and c axes are 2.0(1) × 10^{-3} and 5.5(1) × 10^{-3} GPa^{-1}, which are consistent with the values 1.9487 × 10^{-3} and 5.7588 × 10^{-3} GPa^{-1} from Ross and Reeder (1992). These results confirm that the c axis is two to three times more compressible than the a axis. This same behavior holds at higher temperatures, and the axial compressibilities at 873 K are also reported in Figure 10a. The linear compressibilities of the a and c axes increase with increasing temperature and equal 2.5(2) × 10^{-3} and 6.2(2) × 10^{-3} GPa^{-1} at 873 K, respectively. The structural explanation for the higher compressibility of the c axis in dolomite was discussed by Ross and Reeder (1992).

By applying the same kind of isothermal pressure correction as described for aragonite, we obtain the isobaric mean linear thermal expansivities at different pressures. Figure 10b gives the value of mean linear thermal expansivities at 1 bar obtained by Reeder and Markgraf (1986), as well as our data for 2 and 4 GPa. The anisotropy in the linear thermal expansion ($\alpha_c \approx 2.5\ \alpha_a$) does not seem to be affected by pressure up to 4 GPa.

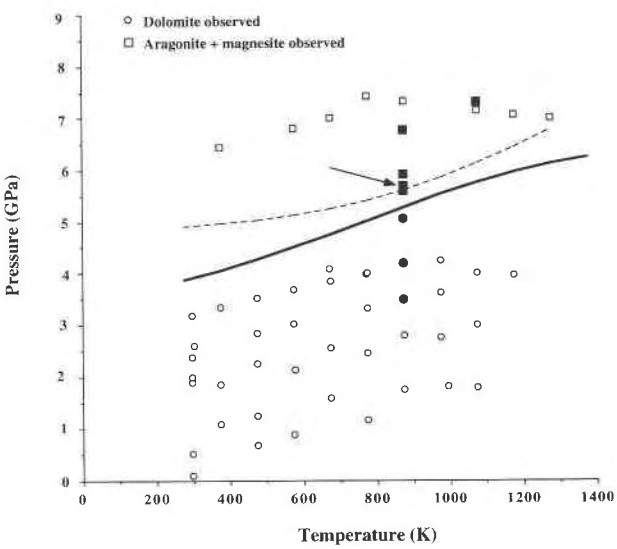

FIGURE 11. Calculated equilibrium curves for the reaction dolomite → aragonite + magnesite, using the EOS measured in this study. Solid line corresponds to the reaction calculated with thermodynamic data reported in Table 8; dashed line, with the thermodynamic data reported in Saxena et al. (1993). Experimental occurrences of dolomite and of aragonite + magnesite are also shown. Open circles stand for dolomite occurrences, open squares for aragonite + magnesite occurrences. Solid symbols correspond to one specific experiment (path 4 in Fig. 2b); the appearance of the assemblage aragonite + magnesite is shown by the arrow.

Thermodynamics of the breakdown reaction of dolomite into aragonite and magnesite

In addition to the determination of the equation of state for dolomite, we also found that dolomite was metastable vs. aragonite and magnesite above 5–6 GPa (see Fig. 4). Using existing calorimetric data and the EOS determined in this study for dolomite and aragonite, and the EOS for magnesite determined by the same technique (Zhang et al. 1994), we computed the thermodynamic equilibrium for the reaction

$$CaMg(CO_3)_2 \rightarrow CaCO_3 + MgCO_3. \quad (8)$$

The Gibbs free energy of reaction, which equals zero at equilibrium, is

$$\Delta_r G^0_{T,P} = \Delta_r G^0_{T,P_0} + \int_{P_0}^{P} \Delta_r V_{T,P}\, dP \quad (9)$$

where $\Delta_r G^0_{T,P_0}$ is the standard Gibbs free energy of reaction at room pressure and high temperature and $\Delta_r V(T, P)$ is the volume of reaction at P and T, determined from the equations of state. $\Delta_r G^0_{T,P_0}$ is given by

$$\Delta_r G^0_{T,P_0} = \Delta_r H^0_{T_0,P_0} + \int_{T_0}^{T} \Delta_r C_{P_T,P_0}\, dT - T\left(\Delta_r S^0_{T_0,P_0} + \int_{T_0}^{T} \frac{\Delta_r C_{P_T,P_0}}{T}\, dT\right) \quad (10)$$

where $\Delta_r H^0_{T_0,P_0}$ and $\Delta_r S^0_{T_0,P_0}$ are the standard enthalpy and entropy of reaction at 298 K, respectively, and $\Delta_r C_{P_T,P_0}$ is the heat capacity of reaction. Different values have been reported for standard enthalpies and entropies of carbon-

ates at 298 K (e.g., Holland and Powell 1990; Saxena et al. 1993), and there are some discrepancies between databases, especially for magnesite (see Table 8). Recent calorimetric measurements of the enthalpy of formation of magnesite have been used here (Chai and Navrotsky 1993). In the case of dolomite, we were careful to use an enthalpy of formation measured for the specific material that we used in this study (i.e., Eugui dolomite) (Chai et al. 1995). The other thermochemical values were taken from Holland and Powell (1990), and all the thermochemical data are summarized in Table 8. In an alternate calculation, we used the data set of Saxena et al. (1993).

The second term on the right side of Equation 9 is obtained by integrating numerically the high-temperature third-order Birch-Murnaghan EOS using our experimental results for dolomite and aragonite and those of Zhang et al. (1994) for magnesite. We also used an analytical form obtained by integrating a Murnaghan EOS (e.g., Fei and Saxena 1986):

$$V(P, T) = V(P_0, T_0)[1 + \alpha(T - T_0)]\left(1 + \frac{K'_{0,T}}{K_{0,T}}P\right)^{-1/K'_{0,T}}. \quad (11)$$

Because of the relatively small pressure range, the difference between the two procedures is negligible (a few joules for $\Delta_r G$). The calculated equilibrium curves are shown in Figure 11. The sensitivity to calorimetric parameters is shown by the difference between the two curves, which were calculated with the use of different calorimetric parameters only. Linear fits lead to P (GPa) = 3.2 + 0.0023T (K) and P (GPa) = 4.2 + 0.0019T (K), using the calorimetric data of Chai and Navrotsky (1993) and Chai et al. (1995) and those of Saxena et al. (1993), respectively. The experimentally observed occurrences of dolomite and of the assemblage aragonite + magnesite in the experiments are also reported in Figure 11. The agreement is good overall, but from our experimental data there is no basis for determining which curve is better. More phase-equilibrium data are needed to resolve this issue; so far our attempts to reverse the reaction in situ at the synchrotron beamline were unsuccessful because of the relatively slow reaction rates. In addition to the use of this reaction for testing consistency of thermodynamic data sets involving solid carbonates, the reaction might be important in the ultra-high-pressure metamorphism of carbonates. Evidence for it remains to be detected in ultra-deep metamorphic rocks or in shocked carbonatitic materials.

Acknowledgments

Yanick Ricard is warmly acknowledged for his help with processing the equation-of-state data. We appreciate the helpful comments of Y. Wang, Y. Meng, and Ph. Gillet, as well as the assistance of M.T. Vaughan, D. Weidner, and F. Guyot during the experiments. We also thank T.J. Holland and A. Christy for their constructive and helpful reviews. The Center for High Pressure Research (CHiPR) is jointly supported by the National Science Foundation (EAR-8920239) and the State University of New York at Stony Brook. The in situ X-ray experiments were performed at the X-17B1 beamline of the Brookhaven National Synchrotron Light Source (NSLS). This is MPI contribution no. 157.

References cited

Anderson, O.L. (1984) A universal equation of state. Journal of Geodynamics, 1, 185–214.

Barber, D.J., Heard, H.C., and Wenk, H.R. (1981) Deformation of dolomite single crystals from 20°C–800°C. Physics and Chemistry of Minerals, 7, 271–286.

Biellmann, C., and Gillet, P. (1992) High-pressure and high-temperature behaviour of calcite, aragonite and dolomite: A Raman spectroscopic study. European Journal of Mineralogy, 4, 389–393.

Biellmann, C., Guyot, F., Gillet, P., and Reynard, B. (1993a) High-pressure stability of carbonates: Quenching of calcite II, high-pressure polymorph of $CaCO_3$. European Journal of Mineralogy, 5, 503–510.

Biellmann, C., Gillet, P., Guyot, F., Peyronneau, J., and Reynard, B. (1993b) Experimental evidence for carbonate stability in the Earth's lower mantle. Earth and Planetary Science Letters, 118, 31–41.

Birch, F. (1966) Compressibility, elastic constants. In Handbook of Physical Constants, 97, 107–173.

——— (1978) Finite strain isotherm and velocities for single-crystal and polycrystalline NaCl at high pressures and 300 K. Journal of Geophysical Research, 83, 1257–1268.

Byrnes, A.P., and Wyllie, P.J. (1981) Subsolidus and melting relations for the join $CaCO_3$-$MgCO_3$ at 10 kbar. Geochimica et Cosmochimica Acta, 45, 321–328.

Canil, D., and Scarfe, C.M. (1990) Phase relations in peridotite + CO_2 systems to 12 GPa: Implications for the origin of kimberlite and carbonate stability in the Earth's upper mantle. Journal of Geophysical Research, 95, 15805–15816.

Chai, L., and Navrotsky, A. (1993) Thermochemistry of carbonate-pyroxene equilibria. Contributions to Mineralogy and Petrology, 114, 139–147.

Chai, L., Navrotsky, A., and Reeder, R.J. (1995) Energetics of Ca-rich dolomite. Geochimica et Cosmochimica Acta, 59, 939–944.

Decker, D.L. (1971) High pressure equation of state for NaCl, KCl and CsCl. Journal of Applied Physics, 42, 3239–3244.

Eggler, D.H. (1978) The effect of CO_2 upon partial melting of peridotite in the system Na_2O-CaO-Al_2O_3-MgO-SiO_2-CO_2 to 35 kb, with an analysis of melting in a peridotite-H_2O-CO_2 system. American Journal of Science, 278, 305–343.

Fei, Y., and Saxena, S.K. (1986) A thermochemical data base for phase equilibria in the system Fe-Mg-Si-O at high pressure and temperature. Physics and Chemistry of Minerals, 13, 311–324.

Fiquet, G., Guyot, F., and Itié, J.-P. (1994) High-pressure X-ray diffraction study of carbonates: $MgCO_3$, $CaMg(CO_3)_2$, and $CaCO_3$. American Mineralogist, 79, 15–23.

Gillet, P. (1993) Stability of magnesite ($MgCO_3$) at mantle pressure and temperature conditions: A Raman spectroscopic study. American Mineralogist, 78, 1328–1331.

Gillet, P., Biellmann, C., Reynard, B., and McMillan, P. (1993) Raman spectroscopic studies of carbonates: Part I. High pressure and high temperature behaviour of calcite, magnesite, dolomite and aragonite. Physics and Chemistry of Minerals, 20, 1–18.

Hazen, R.M., and Finger, L.W. (1982) Comparative crystal chemistry: Temperature, pressure, composition and the variation of crystal structure, 228 p. Wiley Interscience, New York.

Holland, T.J.B., and Powell, R. (1990) An enlarged and updated internally consistent thermodynamic dataset with uncertainties and correlations: The system K_2O-Na_2O-CaO-MgO-MnO-FeO-Fe_2O_3-Al_2O_3-TiO_2-SiO_2-C-H_2-O_2. Journal of Metamorphic Geology, 8, 89–124.

Humbert, P., and Plicque, F. (1972) Propriétés élastiques de carbonates rhomboédriques monocristallins: Calcite, magnésite, dolomie. Comptes Rendus de l'Académie des Sciences de Paris, 275, 391–394.

Irving, A.J., and Wyllie, P.J. (1975) Subsolidus and melting relationships for calcite, magnesite and the join $CaCO_3$-$MgCO_3$ to 36 kb. Geochimica et Cosmochimica Acta, 39, 36–53.

Kalashnikov, N.G., Pavlovski, M.N., Simakov, G.V., and Trunin, R.F. (1973) Dynamic compressibility of calcite-group minerals. Physics of the Solid Earth, 2, 23–29.

Katsura, T., and Ito, E. (1990) Melting and subsolidus phase relations in the $MgSiO_3$-$MgCO_3$ system at high pressures: Implications to evolution of the Earth's atmosphere. Earth and Planetary Science Letters, 99, 110–117.

Kotra, R.K., See, J.H., Gibson, E.K., Horz, F., Cintala, M.J., and Schmidt, R.S. (1983) Carbon dioxide loss in experimentally shocked calcite and dolomite. Lunar Planetary Science, 14, 401–402.

Kraft, S., Knittle, E., and Williams, Q. (1991) Carbonate stability in the Earth's mantle: A vibrational spectroscopic study of aragonite and dolomite at high pressures and temperatures. Journal of Geophysical Research, 96, 17997–18009.

Kushiro, I., Satake, H., and Akimoto, S. (1975) Carbonate-silicate reactions at high pressures and possible presence of dolomite and magnesite in the upper mantle. Earth and Planetary Science Letters, 28, 116–120.

Lange, M.A., and Ahrens, T.J. (1983) Shock-induced CO_2 production from carbonates and a proto-CO_2-atmosphere on the Earth. Lunar and Planetary Science, 14, 419–420.

——— (1986) Shock-induced CO_2 loss from $CaCO_3$: Implications for early planetary atmospheres. Earth and Planetary Science Letters, 77, 409–418.

Martens, R., Rosenhauer, M., and Von Gehlen, K. (1982) Compressibilities of carbonates. In W. Schreyer, Eds., High pressure researches in geoscience, p. 235–238. Schweizerbartsche Verlagsbuchhandlung, Stuttgart, Germany.

Martinez, I., Deutsch, A., Schärer, U., Ildefonse, P., Guyot, F., and Agrinier, P. (1995) Shock recovery experiments on dolomite and thermodynamical calculations of impact induced decarbonation. Journal of Geophysical Research, 100, 15465–15476.

Meng, Y., Weidner, D.J., and Fei, Y. (1993) Deviatoric stress in a quasi-hydrostatic diamond anvil cell: Effect on the volume-based pressure calibration. Geophysical Research Letters, 18, 1147–1150.

Poirier, J.P. (1991) Introduction to the physics of the Earth's interior, 264 p. Cambridge University Press, Cambridge.

Redfern, S.A.T., Wood, B.J., and Henderson, C.M.B. (1993) Static compressibility of magnesite to 20 GPa: Implications for $MgCO_3$ in the lower mantle. Geophysical Research Letters, 20, 2099–2102.

Reeder, R.J. (1983) Crystal chemistry of the rhombohedral carbonates. In R.J. Reeder, Ed., Carbonates: Mineralogy and chemistry, p. 1–47. Mineralogical Society of America, Washington, DC.

Reeder, R.J., and Nakajima, Y. (1982) The nature of ordering and ordering defects in dolomite. Physics and Chemistry of Minerals, 8, 29–35.

Reeder, R.J., and Wenk, H.-R. (1983) Structure refinements of some thermally disordered dolomites. American Mineralogist, 68, 769–776.

Reeder, R.J., and Markgraf, S.A. (1986) High-temperature crystal chemistry of dolomite. American Mineralogist, 71, 795–804.

Ross, N.L. (1994) Magnesite at high pressure. Terra Nova Abstract, Supplement 1, 40.

Ross, N.L., and Reeder, R.J. (1992) High-pressure structural study of dolomite and ankerite. American Mineralogist, 77, 412–421.

Salje, E., and Viswanathan, K. (1976) The phase diagram calcite-aragonite as derived from the crystallographical properties. Contributions to Mineralogy and Petrology, 55, 55–67.

Saxena, S.K., and Zhang, J. (1990) Thermochemical and pressure-volume-temperature systematics of data on solids, example: tungsten and MgO. Physics and Chemistry of Minerals, 17, 45–51.

Saxena, S.K., Chatterjee, N., Fei, Y., and Shen, G. (1993) Thermodynamic data on oxides and silicates, 428 p. Springer-Verlag, Berlin.

Stöffler, D. (1982) Density of minerals and rocks under shock compression. In Numerical data and functional relationships in science and technology, 1, 121–183.

Vizgirda, J., and Ahrens, T.J. (1982) Shock compression of aragonite and implications for the equation of state of carbonates. Journal of Geophysical Research, 87, 4747–4758.

Wallace, M.E., and Green, D.H. (1988) An experimental determination of primary carbonatite magma composition. Nature, 335, 343–346.

Wang, Y., Weidner, D.J., Liebermann, R.C., and Zhao, Y. (1994) *P-V-T* equation of state of $(Mg,Fe)SiO_3$ perovskite: Constraints on composition of the lower mantle. Physics of the Earth and Planetary Interiors, 83, 13–40.

Weidner, D.J., Vaughan, M.T., Ko, J., Wang, Y., Liu, X., Yeganeh-Haeri, A., Pacalo, R.E., and Zhao, Y. (1992) Characterization of stress, pressure and temperature in SAM 85, a DIA type high pressure apparatus. In Y. Syono and M.H. Manghnani, Eds., High pressure research in mineral physics, p. 13–17. American Geophysical Union, Washington, DC.

Weidner, D.J., Wang, Y., and Vaughan, M.T. (1994) Yield strength at high pressure and temperature. Geophysical Research Letters, 21, 753–756.

Williams, Q., Collerson, B., and Knittle, E. (1992) Vibrational spectra of magnesite ($MgCO_3$) and calcite III at high pressures. American Mineralogist, 77, 1158–1165.

Wyllie, P.J., and Huang, W.L. (1976) Carbonation and melting reactions in the system CaO-MgO-SiO_2-CO_2 at mantle pressures with geophysical and petrological implications. Contributions to Mineralogy and Petrology, 54, 79–107.

Zhang, J., Martinez, I., Guyot, F., Gillet, P., and Saxena, S.K. (1994) In situ X-ray diffraction study on magnesite at high pressure and temperature. Eos, 75 (supplement no. 44), 661.

Manuscript received August 15, 1995
Manuscript accepted January 8, 1996